(Supporting Information)

Noble Metal-Free Bimetallic Nanoparticle-Catalyzed Selective Hydrogen Generation from Hydrous Hydrazine for Chemical Hydrogen Storage

Sanjay Kumar Singh, Ashish Kumar Singh, Kengo Aranishi, and Qiang Xu*

National Institute of Advanced Industrial Science and Technology (AIST), Ikeda, Osaka 563-8577, Japan

*Correspondance to Qiang Xu (q.xu@aist.go.jp)

1. Catalyst Preparation

1.1. Chemicals

Commercial chemicals were used as received for catalyst preparation and hydrazine decomposition experiments. Hydrazine monohydrate ($H_2NNH_2 \cdot H_2O$, 98%), sodium borohydride ($NaBH_4$, 99%) and hexadecyltrimethyl ammonium bromide (CTAB, 95%) were obtained from Aldrich. Cobalt(II) chloride hexahydrate ($CoCl_2 \cdot 6H_2O$, 99.5%), nickel(II) chloride hexahydrate ($NiCl_2 \cdot 6H_2O$, 99.9%), iron(II) sulphate heptahydrate ($FeSO_4 \cdot 7H_2O$, 99%) and copper(II) chloride dihydrate ($CuCl_2 \cdot 2H_2O$, 99%) were obtained from Wako. Sodium hydroxide (NaOH, 98%) was obtained from Chameleon Reagent, Japan.

1.2. Syntheses of NiFe, Ni_3Fe and $NiFe_3$ nanocatalysts

The NiFe nanocatalyst was prepared using aqueous-phase surfactant-aided co-reduction process. Typically, 0.024 g of $NiCl_2 \cdot 6H_2O$ and 0.028 g of $FeSO_4 \cdot 7H_2O$ were dissolved in 2.5 mL of distilled water containing 0.100 g of hexadecyltrimethylammonium bromide by vigorous shaking, to which an aqueous solution of sodium borohydride (1.5 mL, 0.010 g) was added. The content of the flask is vigorously shaken to obtain the NiFe nanocatalyst as a black suspension, which was used for the catalytic reaction. The Ni_3Fe and $NiFe_3$ nanocatalysts were prepared using $NiCl_2 \cdot 6H_2O$ and $FeSO_4 \cdot 7H_2O$ in 3:1 (Ni/Fe) and 1:3 (Ni/Fe) molar ratios, respectively, following the analogous process for the NiFe nanocatalyst. The obtained nanocatalysts were washed with water and ethanol and dried in vacuum for characterization.

2. Catalyst characterization

2.1. X-ray photoelectron spectroscopy (XPS)

XPS analyses were carried out on a Shimadzu ESCA-3400 X-ray photoelectron spectrometer using an Mg K source (10 kV, 10 mA). The Ar sputtering experiments were carried out under the conditions of background vaccum 3.4 x 10^{-6} Pa and sputtering acceleration voltage 1 kV.

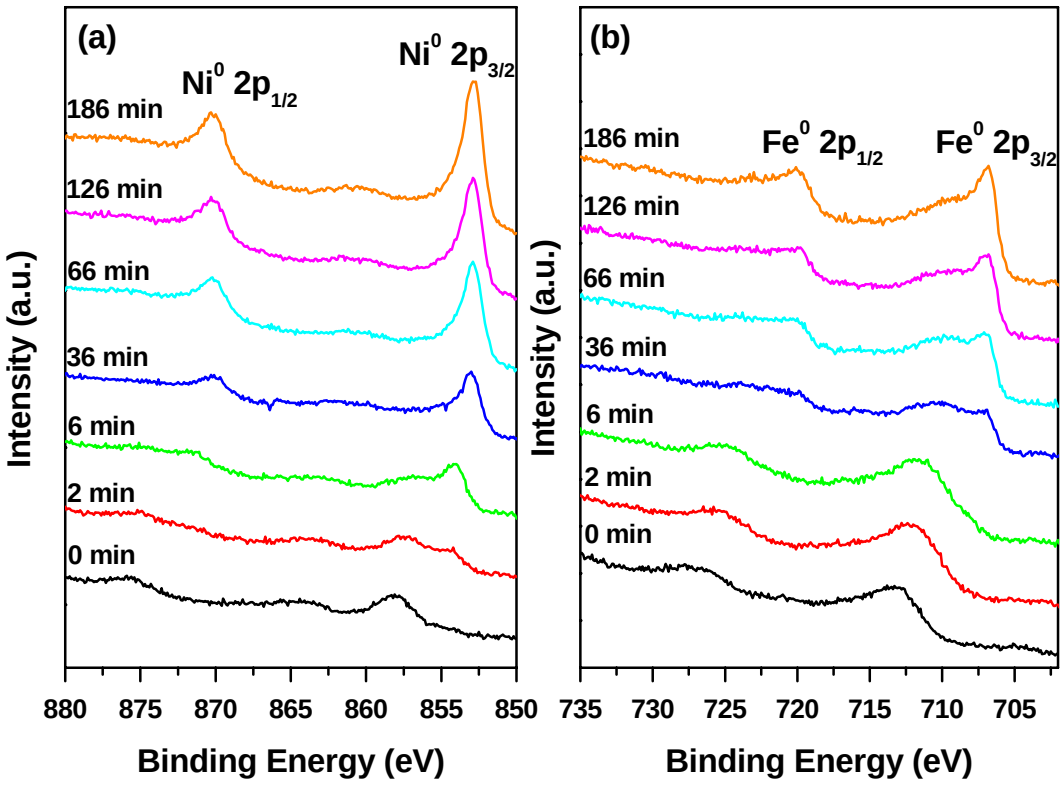

Figure S1. XPS spectra for NiFe nanocatalyst showing (a) Ni $2p_{3/2}$ and $2p_{1/2}$ and (b) Fe $2p_{3/2}$ and $2p_{1/2}$ peaks before and after periodic Ar etching (2 ~ 186 min).

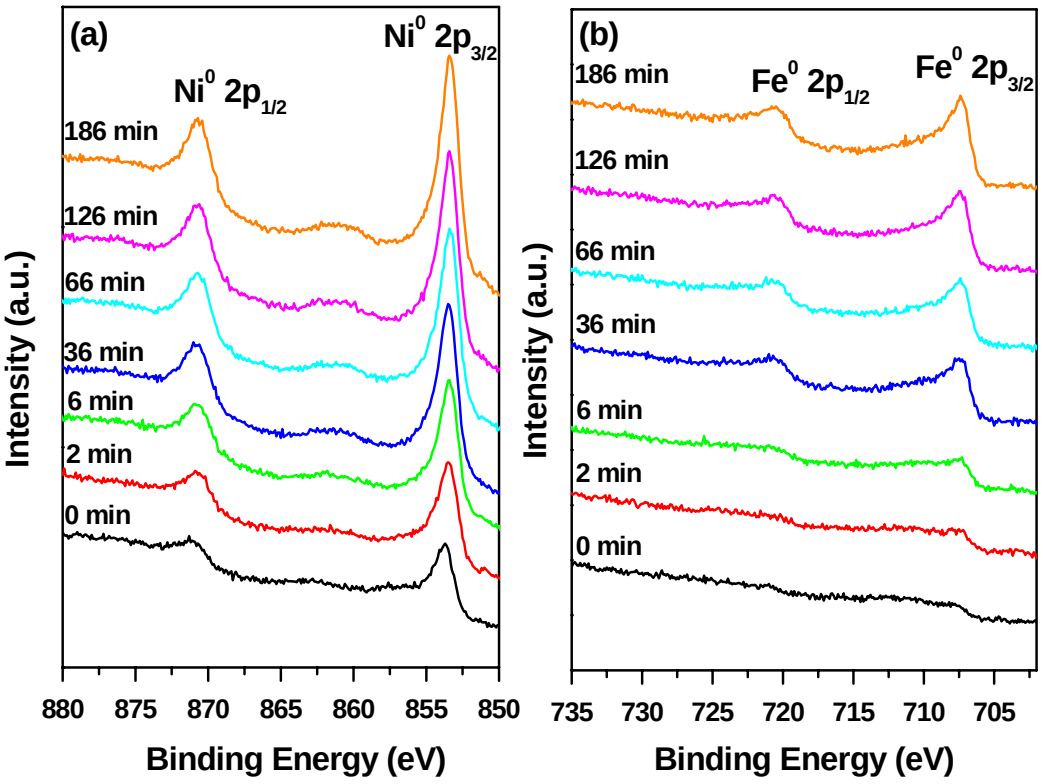

Figure S2. XPS spectra for Ni_3Fe nanocatalyst showing (a) Ni $2p_{3/2}$ and $2p_{1/2}$ and (b) Fe $2p_{3/2}$ and $2p_{1/2}$ peaks before and after periodic Ar etching (2 ~ 186 min).

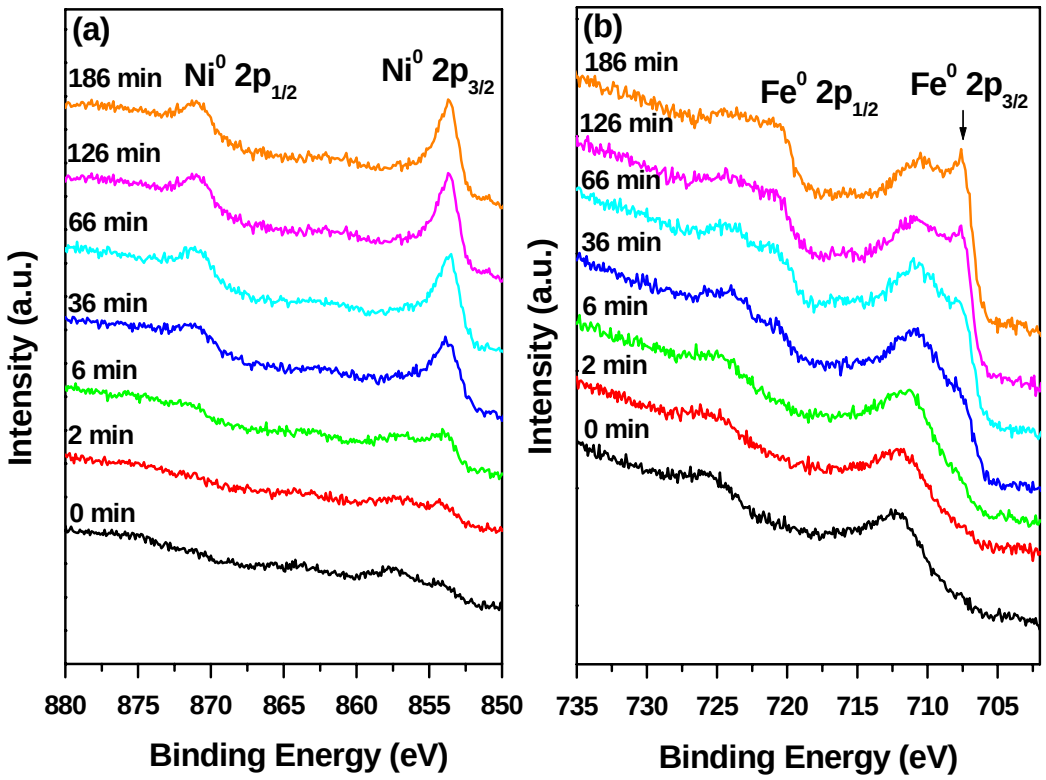

Figure S3. XPS spectra for $NiFe_3$ nanocatalyst showing (a) Ni $2p_{3/2}$ and $2p_{1/2}$ and (b) Fe $2p_{3/2}$ and $2p_{1/2}$ peaks before and after periodic Ar etching (2 ~ 186 min).

2.2. Powder X-ray diffraction (XRD)

XRD was performed on a Rigaku RINT-2000 X-ray diffractometer (Cu Kα). The broad peak in the 2θ range of 42° ~45° shifts towards higher 2θ value with the increase of Ni content in Ni-Fe nanoparticles, suggesting the presence of metallic nickel and iron in alloy form.

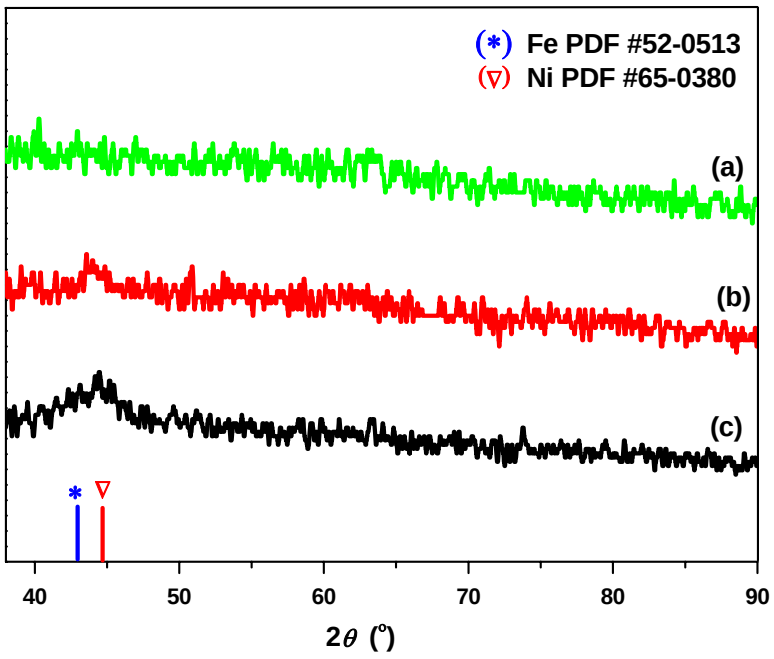

Figure S4. XRD profiles for (a) $NiFe_3$, (b) NiFe and (c) Ni_3Fe nanocatalysts.

2.3. Scanning electron microscopy (SEM) and Transmission electron microscopy (TEM)

Scanning electron microscope (SEM, Hitachi S-5000) and transmission electron microscope (TEM, FEI TECNAI G^2) equipped with energy dispersed X-ray spectroscopy (ESD) detector were applied for the detailed microstructure information of the NiFe catalyst and a transmission electron microscope of JEOL (JEM-3000F) was used for the $NiFe_3$ catalyst. The TEM samples were prepared by depositing few droplets of the nanoparticle suspension onto the amorphous carbon-coated copper grids, which were dried under argon atmosphere.

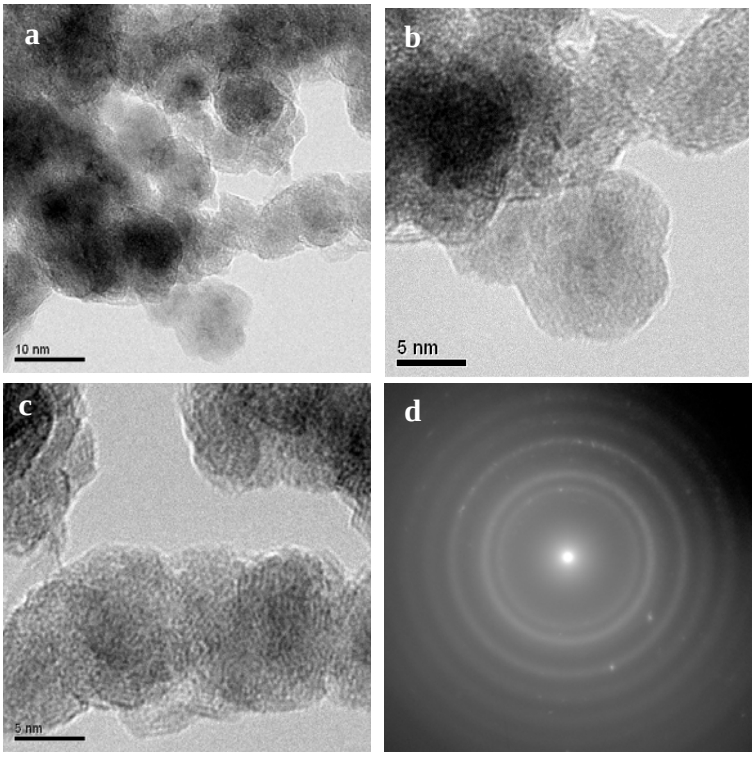

Figure S5. (a-c) TEM images and corresponding (d) SAED from (a) for the NiFe nanocatalyst.

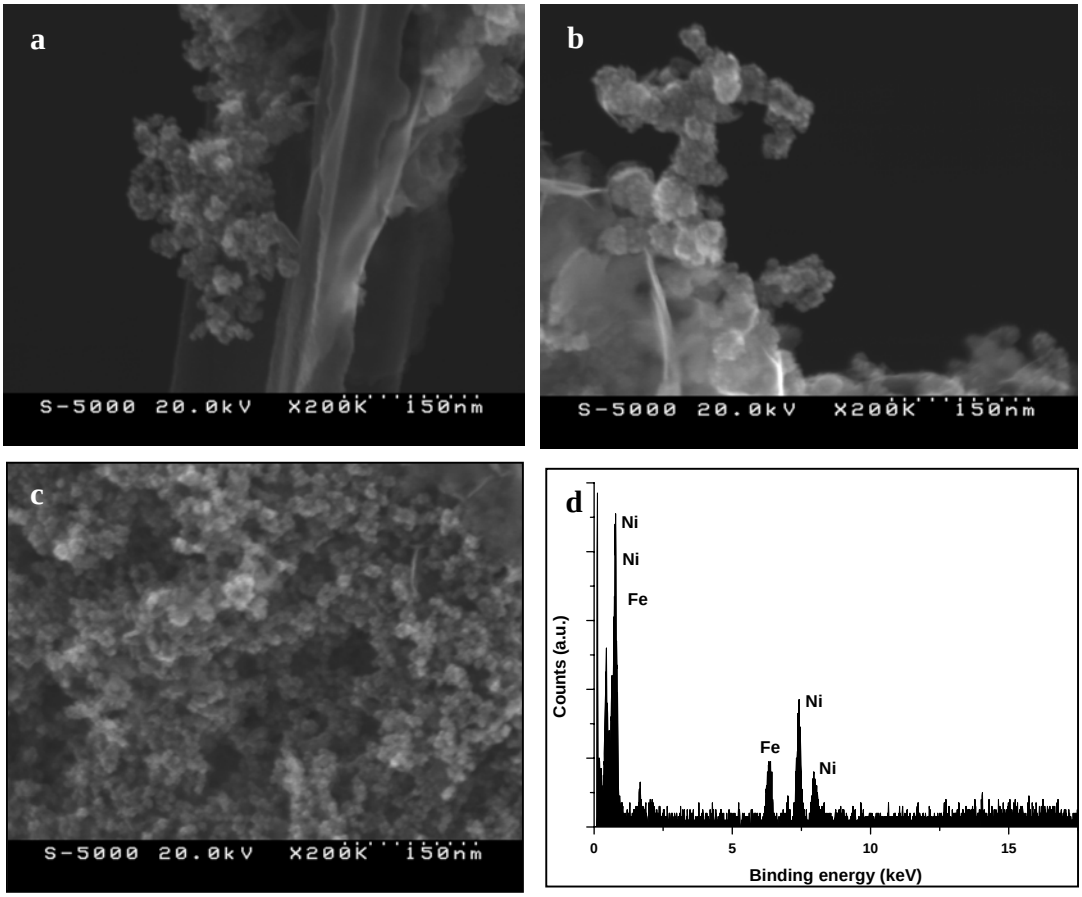

Figure S6. (a-c) SEM images and (d) EDS pattern of the NiFe nanocatalyst.

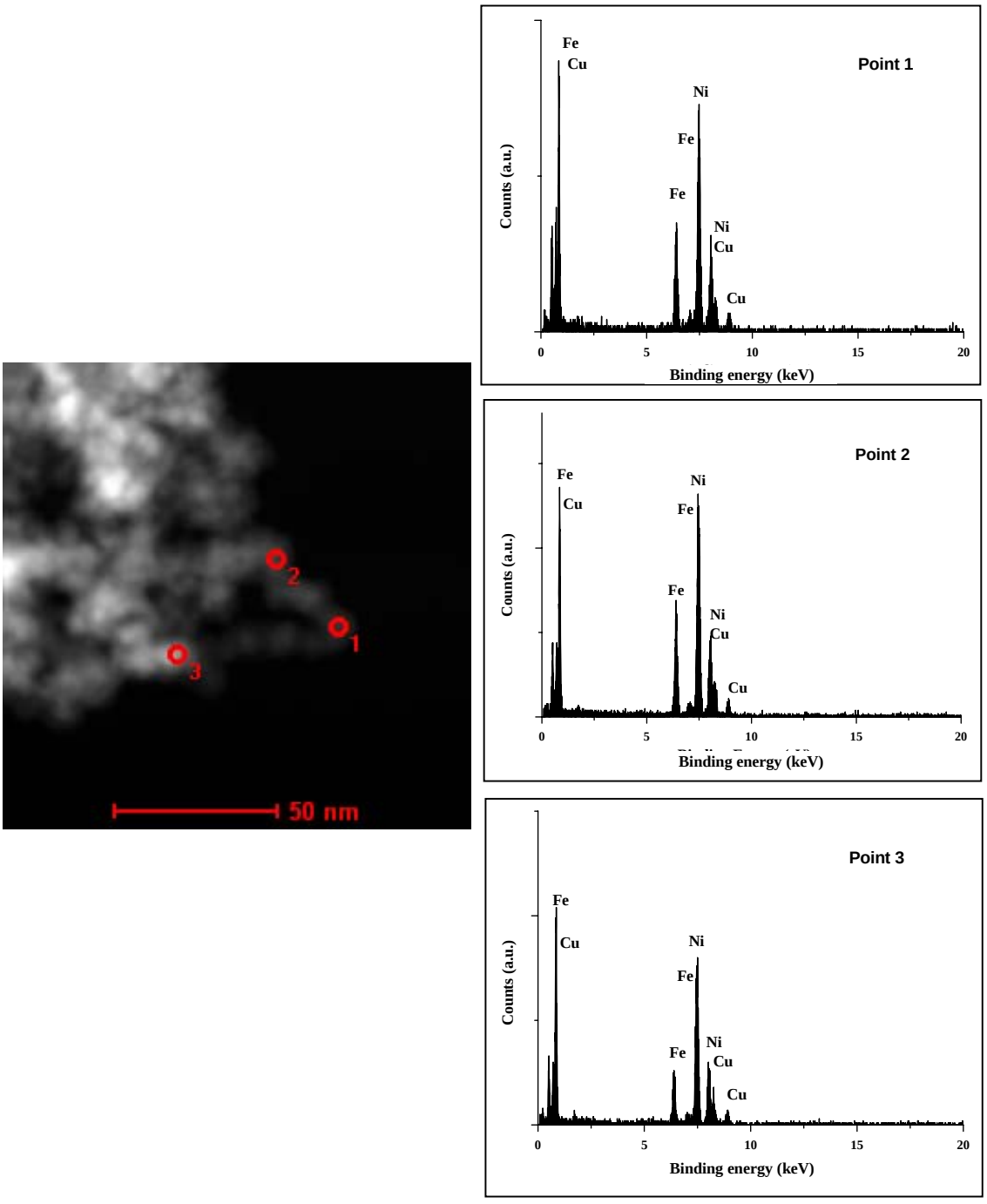

Figure S7. HAADF-STEM image with corresponding EDS profiles at several points for the NiFe nanocatalyst.

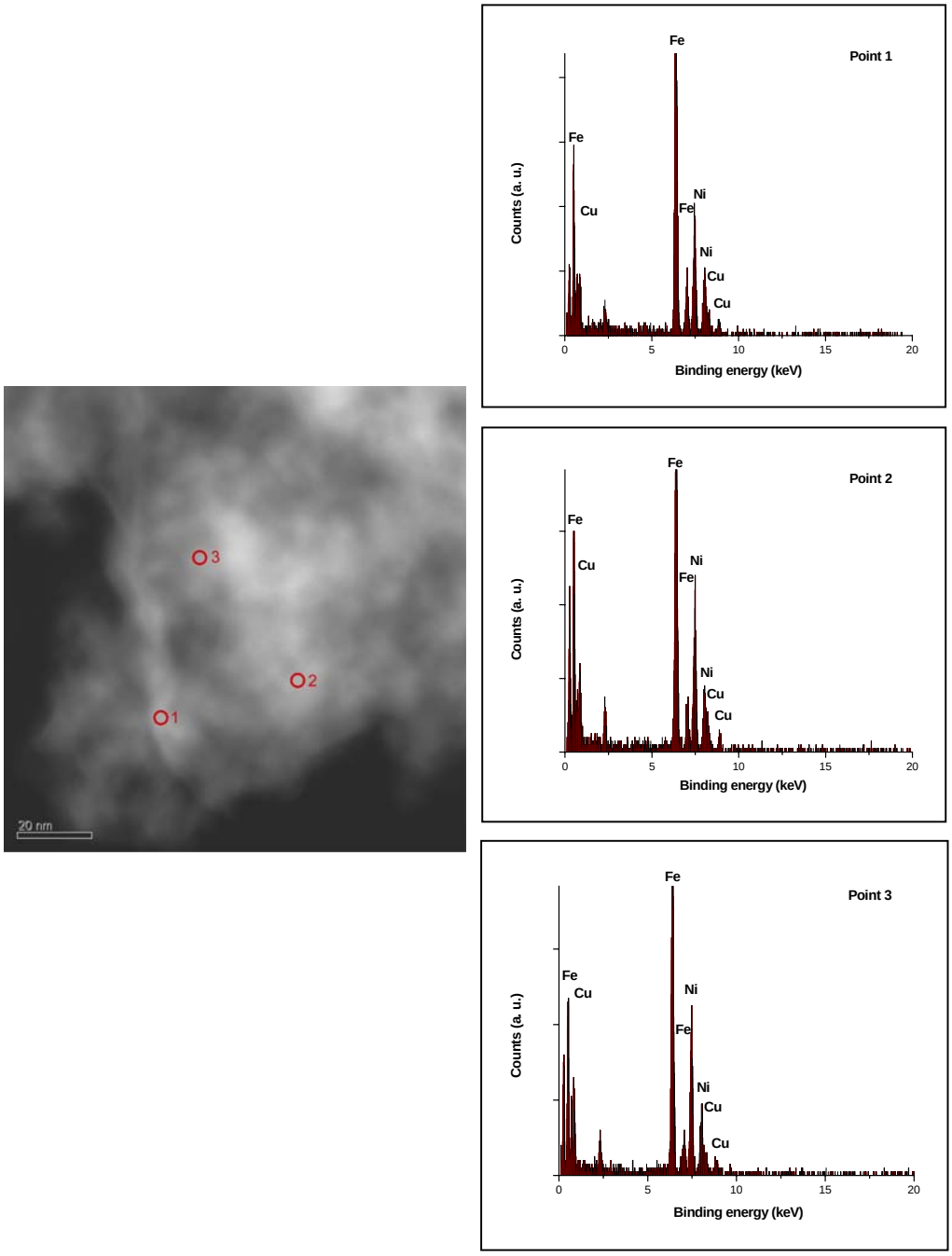

Figure S8. HAADF-STEM image with corresponding EDS profiles at several randomly selected points for the $NiFe_3$ nanocatalyst.

3. Catalytic reactions for hydrous hydrazine decomposition

Catalytic reactions were carried out following our previously reported method.[S1,S2] Typically, 2.0 mmol of hydrazine monohydrate was injected to the glass reactor containing an aqueous suspension of nanocatalysts to initiate the catalytic decomposition reaction of hydrous hydrazine. The reaction temperature was kept constant at a specified reaction temperature using a water bath. The gas released during the reaction was passed though a hydrochloric acid solution (1.0 M) before measured volumetrically.

Table S1. pH values of the solution at different steps of the preparation of the NiFe catalyst and the decomposition of hydrous hydrazine over this catalyst

Step	Condition	pH
1	Before reduction of metals	5.7
2	After reduction by $NaBH_4$	7.6
3	After addition of NaOH (0.5 M)	12.7
4	After addition of $H_2NNH_2 \cdot H_2O$ (2 mmol)	12.9
5	After release of 3.0 equivalent of gases	12.7

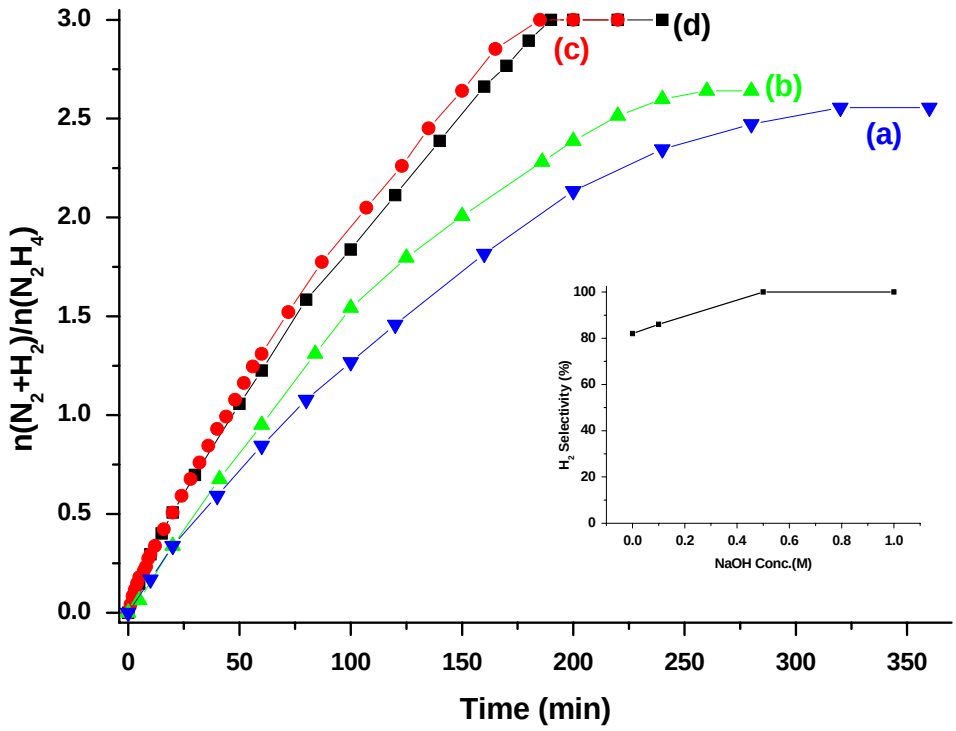

Figure S9. Time course plots for the decomposition of hydrous hydrazine (0.5 M) to hydrogen in the presence of NiFe nanocatalyst (a) without NaOH and with NaOH of (b) 0.1 M, (c) 0.5 M and (d) 1.0 M (catalyst/H_2NNH_2 = 1:10) at 343 K (*Inset* shows the effect of NaOH concentration on H_2 selectivity).

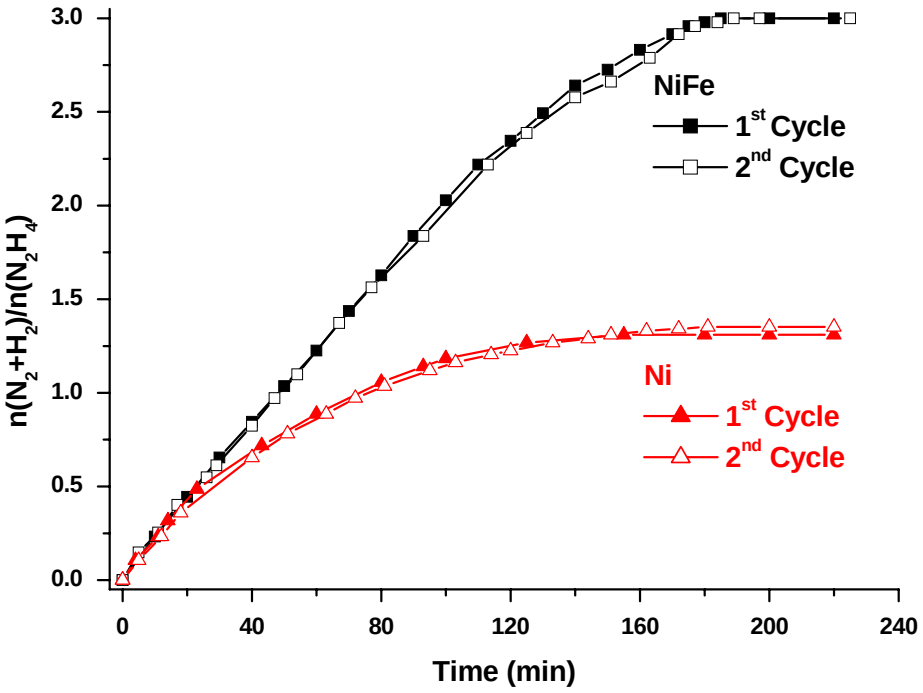

Figure S10. Time course plots for the decomposition of hydrous hydrazine (0.5 M) to hydrogen in the presence of NiFe (black) and Ni (red) catalysts with NaOH (0.5 M) at 343 K. The 2nd cycle reaction was performed by subsequently adding another equivalent of hydrous hydrazine. For both of the NiFe and Ni catalysts, the gas release rates and H_2 selectivities during the 1st and 2nd cycles kept unchanged, indicating that the $(N_2+H_2)/NH_3$ ratios are constant over the course of reaction and the catalysts have high stability.

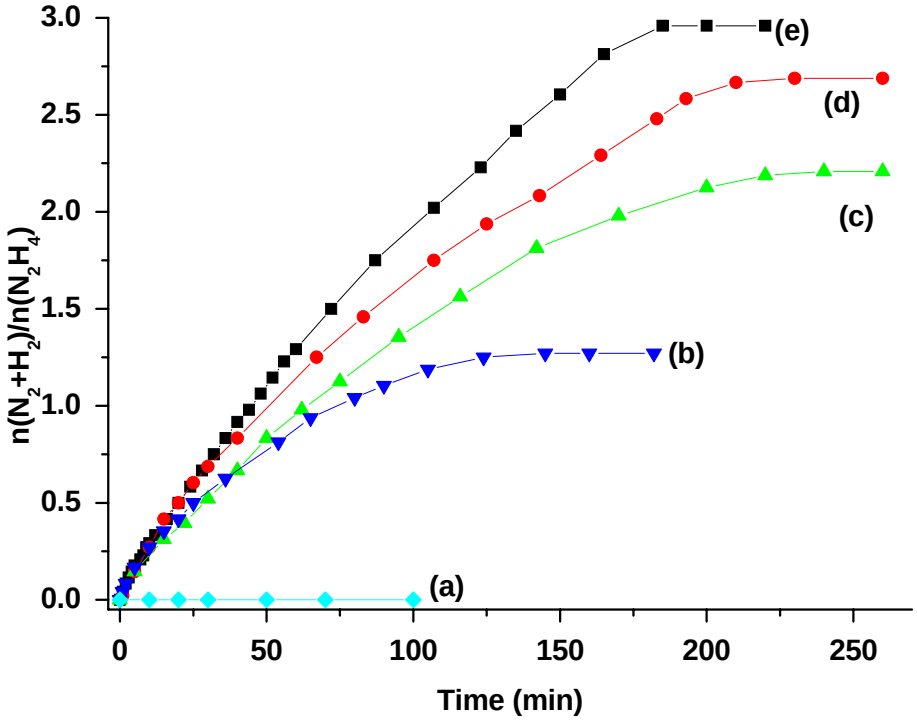

Figure S11. Time course plots for the decomposition of hydrous hydrazine (0.5 M) to hydrogen in the presence of (a) Fe, (b) Ni, (c) $NiFe_3$, (d) Ni_3Fe and (e) NiFe nanocatalysts (catalyst/H_2NNH_2 = 1:10) with NaOH (0.5 M) at 343 K.

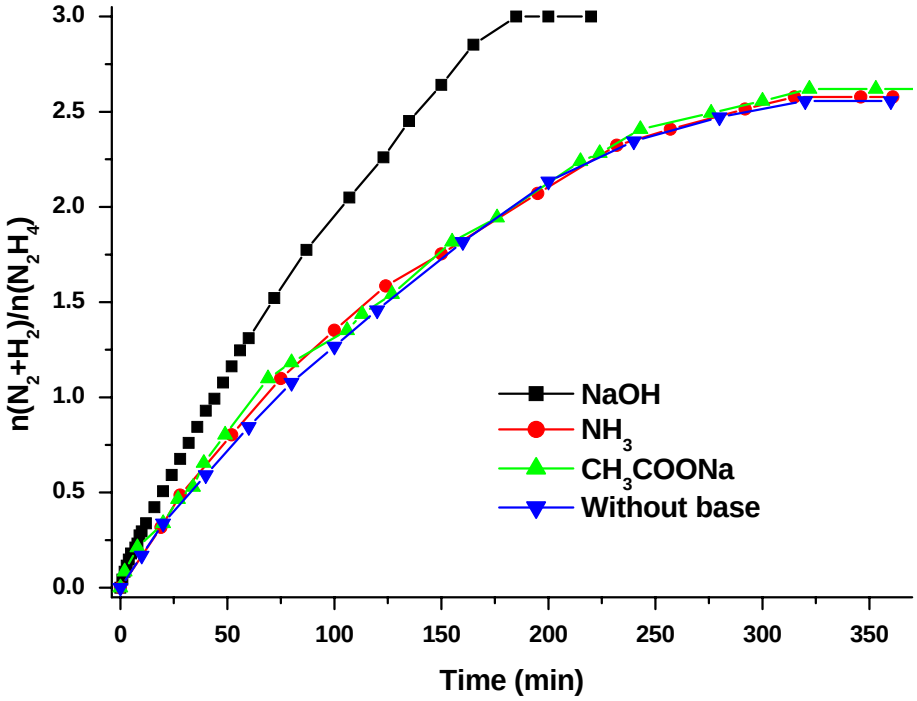

Figure S12. Time course plots for the decomposition of hydrous hydrazine (0.5 M) to hydrogen in the presence of NiFe nanocatalyst with different bases at 343 K.

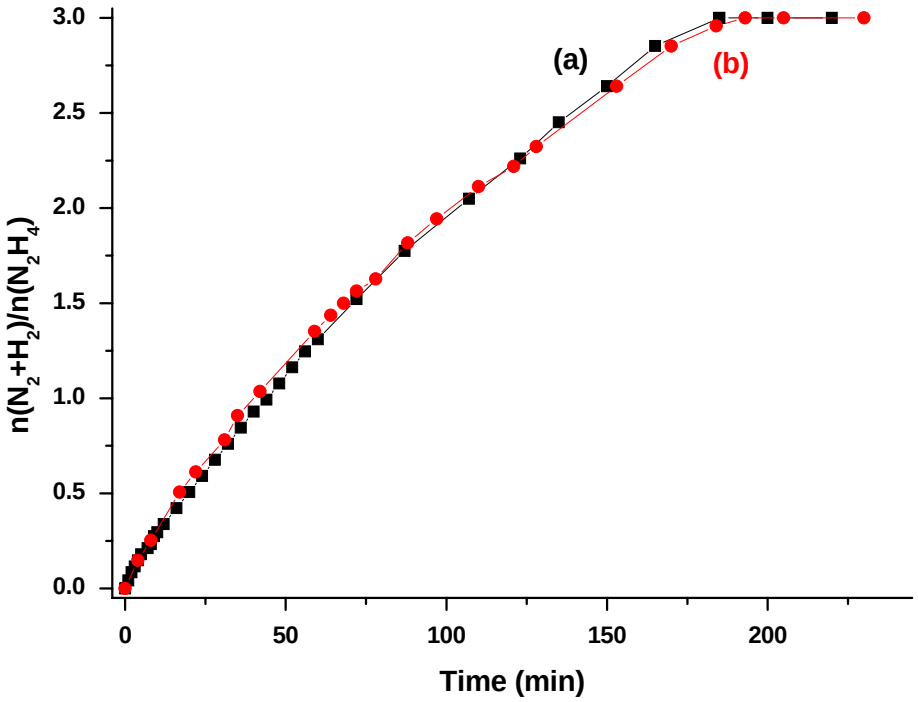

Figure S13. Time course plots for the decomposition of hydrous hydrazine (0.5 M) to hydrogen over the NiFe catalyst (a) without NH_3 and (b) with NH_3 (0.5 M) in the presence of 0.5 M NaOH at 343 K.

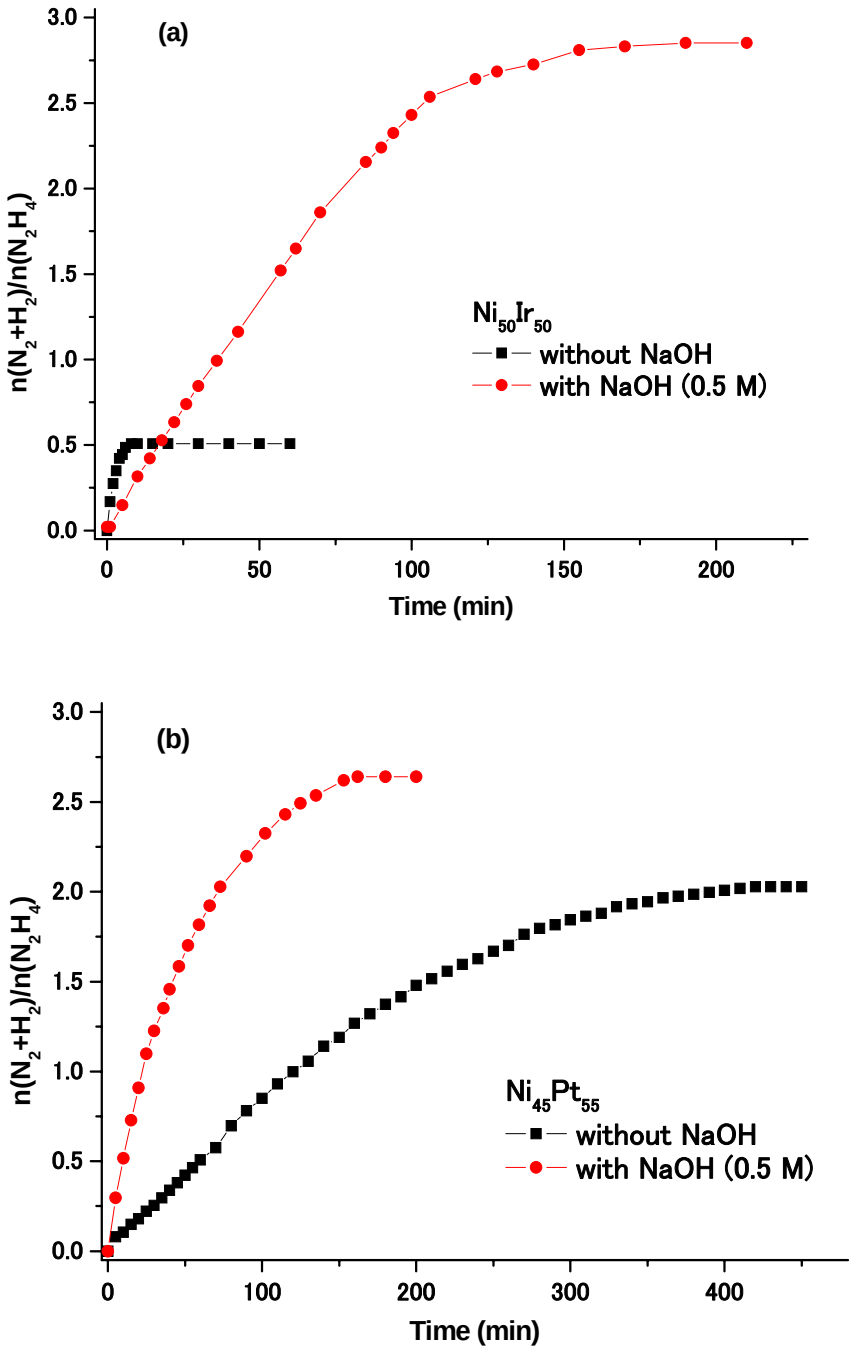

Figure S14. Time course plots for the decomposition of hydrous hydrazine (0.5 M) to hydrogen in the presence of (a) $Ni_{50}Ir_{50}$ and (b) $Ni_{45}Pt_{55}$ nanocatalysts with and without NaOH (0.5 M) at 298 K.

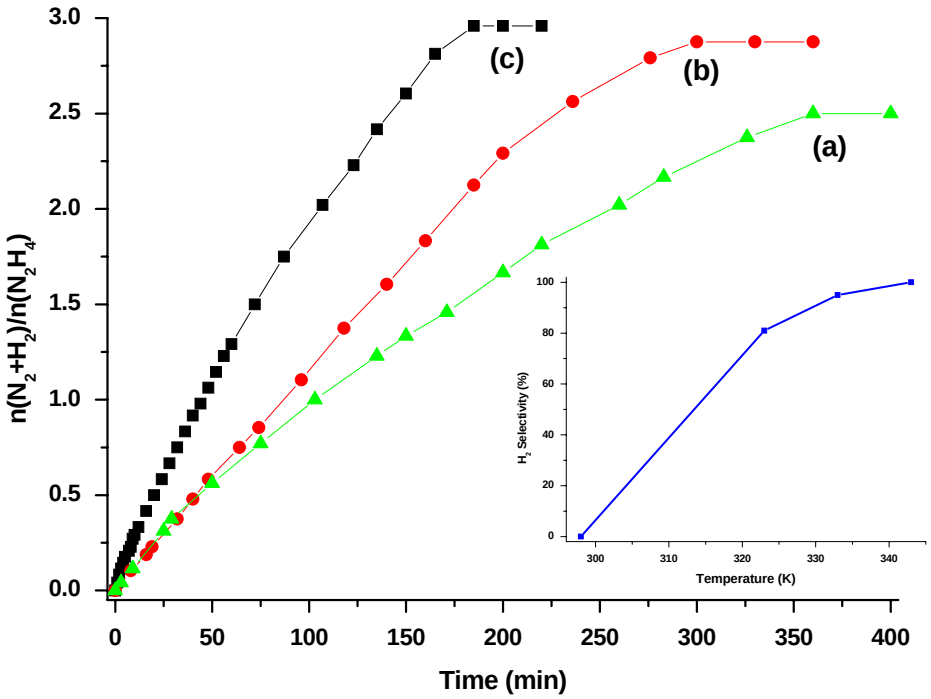

Figure S15. Time course plots for the decomposition of an aqueous solution of hydrazine (0.5 M) to hydrogen in the presence of NiFe catalyst (catalyst/H_2NNH_2 = 1:10) with NaOH (0.5 M) at (a) 323 K, (b) 333 K and (c) 343 K (*Inset* shows the effect of temperature on H_2 selectivity).

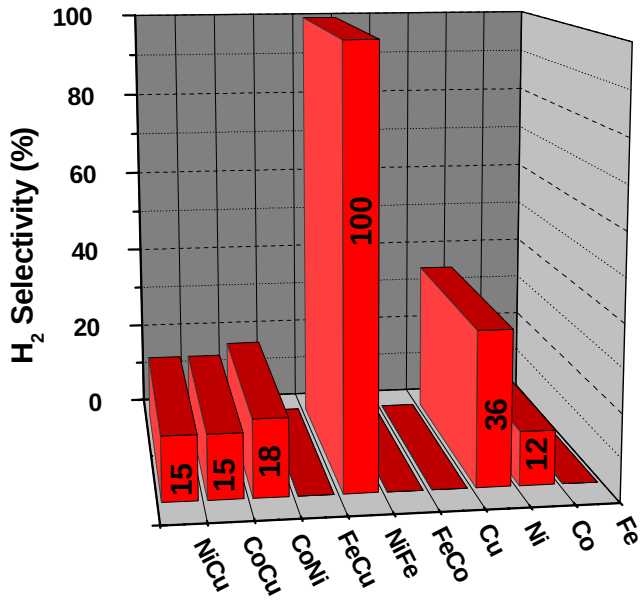

Figure S16. Comparative H_2 selectivity in the decomposition of hydrous hydrazine (0.5 M) to hydrogen in the presence of monometallic (Fe, Co, Ni and Cu) and bimetallic (FeCo, NiFe, FeCu, CoNi, CoCu and NiCu) nanocatalysts (catalyst/H_2NNH_2 = 1:10) with NaOH (0.5 M) at 343 K. These nanocatalysts were prepared under analogous condition as for the NiFe nanocatalyst using respective metal salts.

4. Magnetic recycle of the catalyst

Employing magnetic nanoparticles as the catalyst intrinsically holds the advantage of its easy separation by a magnet. The NiFe nanocatalyst suspended in the aqueous solution (a) as black particles can be effectively aggregated and separated from the solution by a magnet as shown in (b) (Figure S17). This easy magnetic separation is greatly useful for the recycle application of the catalyst.

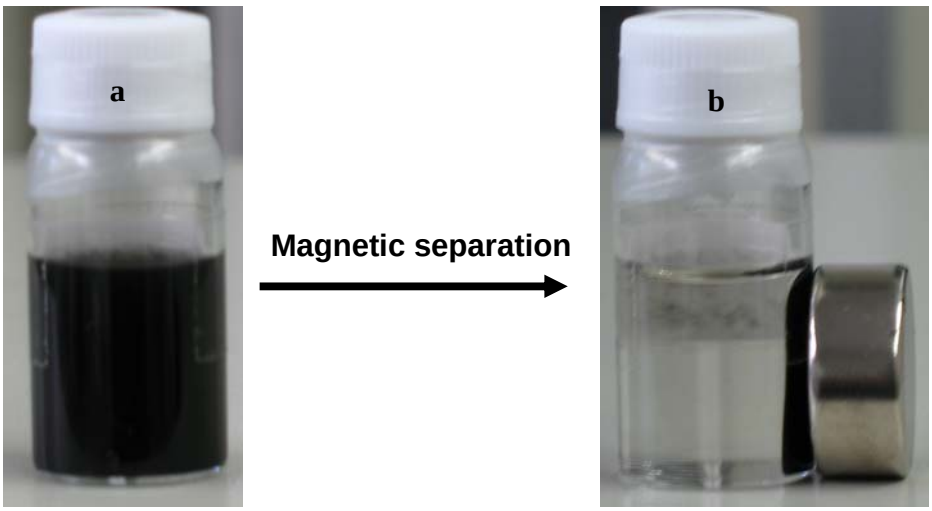

Figure S17. Photographs of the Ni-Fe NPs (a) before and (b) after magnetic separation.

References

(S1) Singh, S. K.; Zhang, X.-B.; Xu, Q. *J. Am. Chem. Soc.* **2009**, *131*, 9894-9895.

(S2) (a) Singh, S. K.; Xu, Q. *J. Am. Chem. Soc.* **2009**, *131*, 18032-18033. (b) Singh, S. K.; Xu, Q. *Inorg. Chem.* **2010**, *49*, 6148-6152. (c) Singh, S. K.; Xu, Q. *Chem. Commun.* **2010**, 6545-6547.